582 *Biochemistry* **2010,** *49,* 582–590
DOI: 10.1021/bi901435q

BIOCHEMISTRY
including biophysical chemistry & molecular biology
Article

pH-Dependent Conformational Changes in Tear Lipocalin by Site-Directed Tryptophan Fluorescence[†]

Oktay K. Gasymov, Adil R. Abduragimov, and Ben J. Glasgow*

Departments of Pathology and Ophthalmology, UCLA School of Medicine, Jules Stein Eye Institute, 100 Stein Plaza, Los Angeles, California 90095

Received August 15, 2009; Revised Manuscript Received December 17, 2009

ABSTRACT: Tear lipocalin (TL), a major protein of human tears, binds a broad array of endogenous ligands. pH-dependent ligand binding in TL may have functional implications in tears. Previously, conformational selections of the AB and GH loops have been implicated in ligand binding by site-directed tryptophan fluorescence (SDTF). In this study, SDTF was applied to the AB and GH loops to investigate pH-driven conformational changes relevant to ligand binding. Both loops demonstrate significant but distinct conformational rearrangements over a wide pH range. In the low-pH transition, from 7.3 to 3.0, residues of the GH loop exhibit decreased solvent accessibilities. In acrylamide quenching experiments, the average quenching rate constant (k_q, accessibility parameter) of the residues in the GH loop is decreased ~38%, from 2.1×10^9 to 1.3×10^9 M^{-1} s^{-1}. However, despite the significant changes in accessibilities for some residues in the AB loop, the average accessibility per residue remained unchanged (average k_q = 1.2 M^{-1} s^{-1}). Accordingly, the low-pH transition induces conformational changes that reshuffle the accessibility profiles of the residues in the AB loop. A significant difference in the titration curves between the holo and apo forms of the W28 mutant suggests that the protonation states of the residues around position 28 modulate conformational switches of the AB loop relevant to ligand binding.

Tear lipocalin (TL),[1] also known as von Ebner's gland protein, is a prominent member of the lipocalin family. As a typical lipocalin, TL possesses a ligand binding barrel that consists of eight antiparallel β- strands with a repeated +1 topology (*1*). The solution structure of TL, determined by site-directed tryptophan fluorescence (SDTF), has revealed a capacious cavity (*2*). These findings have subsequently been verified by crystallography (*3*).

TL is the principal lipid binding protein in tears and the second most abundant protein by molarity. TL binds a broad array of endogenous ligands that include an assortment of fatty acids, alkyl alcohols, glycolipids, phospholipids, and cholesterol (*4*). Numerous putative functions have been suggested for TL. These are scavenging lipid from the corneal surface to prevent the formation of lipid-induced dry spots (*5*), solubilization of lipids in tears (*2*), antimicrobial activity (*6*), cysteine proteinase inhibition (*7*), transport of sapid molecules in saliva (*8*), transport of retinol in tears (*9*), scavenging potentially harmful lipid oxidation products (*10*), transport of antioxidants in tears (*11*), and endonuclease activity (*12*).

Because all putative functions of TL are linked to various ligands, molecular mechanisms of ligand binding are of considerable interest. Commonly, a single binding site is presumed for binding of a ligand to a protein. TL demonstrates a different motif. Spin-labeled analogues of fatty acids have been used to determine the orientation of fatty acids in the cavity of TL. Fatty acids are oriented with the hydrocarbon tail buried in the cavity and the carboxyl group oriented toward the mouth (*13*, *14*). However, TL can also interact, although relatively weakly, with fatty acids oriented in the opposite direction. SDTF was applied to measure the ligand binding energy landscape of TL (*15*). Palmitic acid does not have a single position but is distributed asymmetrically in the cavity of TL. Experimental data suggest that the ligand binding selects the excited protein states, which originate primarily from conformational selections of the AB and GH loops (*15*). The AB and GH loops are not resolved in the crystal structure (*3*). Since the crystal structure of TL was determined at 100 K, the low electron density observed for the AB and GH loops most likely arises from the trapped conformational substates, whose coordinates deviate significantly from each other.

In binding of the protein to small ligands, a population shift to the active conformations (excited protein states) rather than an induced fit mechanism is dominant (*16*). This mechanism was also suggested for binding of fatty acids to β-lactoglobulin, which belongs to the lipocalin family. It has been well documented that the active conformation of β-lactoglobulin originates from fluctuation of the protonation states of Glu89 that create open or closed forms of the protein (*17*−*21*). Therefore, the conformational states of β-lactoglobulin can be modulated by changing the pH of the solution.

Changes in pH, along with those in temperature, pressure, and chemical milieu, are widely employed to populate excited protein states. In addition, pH-dependent ligand binding may be functionally important for TL because the tear film is replete with

[†]Supported by U.S. Public Health Service Grants (National Institutes of Health) EY11224 and EY00331 as well as the Edith and Lew Wasserman Endowed Professorship in Ophthalmology.

*To whom correspondence should be addressed: Departments of Pathology and Ophthalmology, UCLA School of Medicine, Jules Stein Eye Institute, 100 Stein Plaza, Room B269, Los Angeles, CA 90095. Phone: (310) 825-6998, Fax: (310) 794-2144. E-mail: bglasgow@mednet.ucla.edu.

[1]Abbreviations: IRF, instrument response function; SDTF, site-directed tryptophan fluorescence; TL, human tear lipocalin.

 Published on Web 12/21/2009

negatively charged lipids that potentially create a steep pH gradient at lipid−water interfaces (*22*). pH-driven structural rearrangements as well as perturbations in ligand binding have been shown for TL (*23*−*26*). pH-dependent ligand binding has been demonstrated for other lipocalins, such as retinol binding protein (*27*, *28*), nitrophorin (*29*), and the membrane enzyme PagP (*30*). Conformational rearrangements, mainly involving the loops at the open end of the calyx, are considered to be a general feature of the ligand binding mechanism of the lipocalins (*21*).

Despite the fact that above-mentioned lipocalins share the same pH-dependent feature in ligand binding, details of the molecular actions and outcomes are different. In TL, the movement of the opposing CD and EF loops, which influence the ligand binding, is regulated by pH (*24*). However, application of SDTF to TL reveals that the GH and AB (the longest loop in the lipocalin family) loops have decisive roles in ligand binding. Also, these loops have been thought to participate in both conformational selection of the excited protein states and direct interaction with the ligand (*15*).

In this study, SDTF was applied to the AB and GH loops for investigation of pH-driven conformational changes. Both loops, AB and GH, of TL demonstrate significant conformational rearrangements over a wide pH range. Saturation of TL with palmitic acid alters pH-induced conformational changes for some tested positions. These imply that fluctuations between protonated and unprotonated states of amino acids of TL induce conformational changes necessary for ligand binding.

MATERIALS AND METHODS

Materials. Acrylamide and other chemicals used to prepare various buffers were purchased from Sigma-Aldrich (St. Louis, MO).

Site-Directed Mutagenesis and Plasmid Construction. The TL cDNA in PCR II (Invitrogen), previously synthesized (*31*), was used as a template to clone the TL gene spanning bases 115−592 of the previously published sequence (*9*) into pET 20b (Novagen, Madison, WI). Flanking restriction sites for NdeI and BamHI were added to produce the native protein sequence as found in tears but with the addition of an initiating methionine (*32*). To construct mutant proteins with a single tryptophan, the previously well-characterized TL mutant, W17Y, was prepared with oligonucleotides (Universal DNA Inc., Tigard, OR) by sequential PCR steps (*33*, *34*). Using this mutant as a template, mutant cDNAs were constructed in which selected amino acids were additionally substituted with tryptophan or cysteine. Amino acid 1 corresponds to His, bases 115−118 according to Redl (*9*).

To characterize pH-induced conformational transitions in TL, 17 single-Trp mutants that cover the AB and GH loops at the open end of the cavity were tested (Figure 1). The W17Y mutant, which has been characterized previously (*34*), was used as a template. Single-Trp mutants of TL include W17Y/D25W (for the sake of simplicity denoted as W25), W17Y/R26W (W26), W17Y/E27W (W27), W17Y/F28W (W28), W17Y/P29W (W29), W17Y/E30W (W30), W17Y/M31W (W31), W17Y/N32W (W32), W17Y/L33W (W33), W17Y/E34W (W34), W17Y/S35W (W35), W17Y/V36W (W36), W17Y/T37W (W37), W17Y/H106W (W106), W17Y/G107W (W107), W17Y/K108W (W108), and W17Y/P109W (W109). All mutant proteins have the native fold, which has previously been characterized by far-UV circular dichroism. In addition, all mutant proteins exhibit similar ligand binding properties, which is the principal function of native TL in tears (*15*).

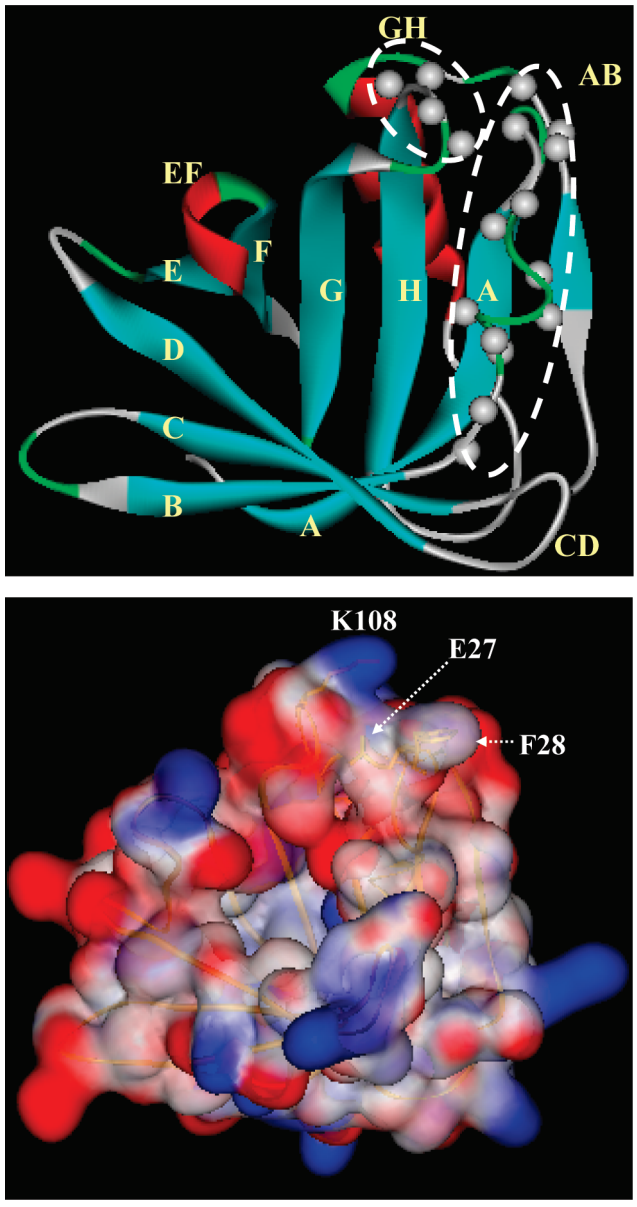

FIGURE 1: Positions of the residues in the AB and GH loops that were sequentially substituted with Trp for examination of pH-induced conformational changes in TL. Gray spheres show locations of the C_α atoms of the amino acid residues. Dashed lines encompass the inspected loop regions. Single and double letters denote the identities of the β-strands and loops, respectively. The ribbon diagram (blue for β-strands, red for α-helix, green for turns, and gray for loops) of TL was generated from Protein Data Bank entry 1XKI with DS Visualizer 2.0 (Accelrys Inc.). Missing loop fragments (part of the AB and GH loops) were modeled using DeepView/Swiss-PdbViewer version 3.7 (GlaxoSmithKline R&D) in accord with solution structure data (*2*). The bottom panel is a surface representation of tear lipocalin, in the same orientation as in the top panel (colored according to the electrostatic potential, blue for positive charge and red for negative).

Expression and Purification of Mutant Proteins. The mutant plasmids were transformed in *Escherichia coli* BL21(DE3), and cells were cultured and proteins expressed, purified, and analyzed as described previously (*2*, *24*). The expressed mutant proteins were used as apoproteins. To obtain the holoproteins, apoproteins were enriched with palmitic acid (1:2).

Absorption Spectroscopy. UV absorption spectra were recorded at room temperature using a Shimadzu UV-2400PC spectrophotometer.

CD Spectral Measurements. Spectra were recorded (Jasco 810 spectropolarimeter, 0.2 and 10 mm path lengths for far- and near-UV spectra, respectively) using protein concentrations of 1.2 mg/mL in 10 mM sodium phosphate (pH 7.5−5.5) or 30 mM sodium citrate (pH 4.0−3.0). Eight and sixteen scans from 190 to 260 nm and from 250 to 320 nm, respectively, were averaged. Results were recorded in millidegrees and converted to mean residue ellipticity in degrees square centimeters per decimole.

The biuret and the Lowry methods were used to determine protein concentrations of stock and dilute solutions, respectively (*35*, *36*).

Steady-State Fluorescence Spectroscopy. Steady-state fluorescence measurements were taken on a Jobin Yvon-SPEX (Edison, NJ) Fluorolog tau-3 spectrofluorometer, and the bandwidths for excitation and emission monochromators were 2 and 3 nm, respectively. An excitation λ of 295 nm was used to ensure that fluorescence was emitted from only the tryptophanyl groups. Protein solutions with an OD of ~0.05 at 295 nm were analyzed. All spectra were from samples in 10 mM sodium phosphate (pH 7.5−5.5) or 30 mM sodium citrate (pH 4.0−3.0) at room temperature. The fluorescence spectra were corrected for light scattering from buffer. Each fluorescence λ_{max} value was determined as an average of five measurements.

Fluorescence Lifetime Measurements. The fluorescence intensity decays were measured using a LaserStrobe fluorescence lifetime instrument (Photon Technology International, Inc., Birmingham, NJ), which consists of a nitrogen laser (GL-3300) linked to a dye laser (GL 302), a frequency doubler (GL 303), and a stroboscopic detector. Laser light with a wavelength of 295 nm was obtained from frequency doubling of 590 nm light using a Rhodamine 6G (Exciton, Inc., Dayton, OH) dye solution. The 295 nm pulses (fwhm ~ 1.5 ns) were used for the excitation of the single-Trp mutants. The decay curves were analyzed at the wavelengths of the respective emission maxima. The emission monochromator slit was 3−5 nm. All measurements were conducted at room temperature. The IRF was determined by measuring scattered light from a solution of glycogen. A DPU-15 optical depolarizer (Optics for Research, Caldwell, NJ) was placed before the emission monochromator to eliminate the polarization dependence of the detection train. Each data point on a lifetime decay curve represents the average of at least nine laser flashes, and each decay represents 300 of these data points evenly spaced over the collection time interval.

The fluorescence intensity decay data were analyzed by the multiexponential decay law, using the software supplied with the PTI instrument:

$$I(t) = \sum \alpha_i \exp(-t/\tau_i)$$

where I is fluorescence intensity and α_i and τ_i are the normalized preexponential factors and decay times, respectively. The amplitude-averaged lifetime $\langle\tau\rangle$ and the intensity-averaged lifetime τ^{av} were calculated as $\langle\tau\rangle = \sum_i \alpha_i\tau_i$ and $\tau^{av} = \sum_i f_i\tau_i$, respectively. f_i, the fractional contribution of each lifetime component to steady-state fluorescence intensity, is defined as $f_i = \frac{\alpha_i\tau_i}{\sum_j \alpha_j\tau_j}$

Accessibility of the Trp Side Chain by Acrylamide Quenching of Fluorescence. The fluorescence of a protein, monitored at the emission maximum λ_{max}, was quenched by the progressive addition of small aliquots of an 8 M acrylamide solution as described previously (*37*). Corrections for dilution of the sample and for inner filter effects caused by acrylamide absorption were performed as previously described (*38*). The quenching data were fit to the modified form of the Stern−Volmer relationship (*38*): $F_0/F = (1 + K_{SV}[Q])e^{V[Q]}$, where F_0 and F are the fluorescence intensities in the absence and presence of the quencher, respectively, [Q] is the concentration of the quencher, V is the apparent static quenching constant (quenching sphere of action), and K_{SV} is the dynamic quenching constant ($K_{SV} = k_q\tau^{av}$, where k_q is bimolecular collisional rate constant and τ^{av} is the intensity-averaged fluorescence lifetime in the absence of the quencher). It has been shown that the intensity-averaged fluorescence lifetime should be used to calculate the average collisional quenching constant when the fluorophore displays multiexponential decay (*39*, *40*). The derived equation for the ratio of the amplitude-averaged lifetimes in quenching is

$$\frac{\langle\tau_0\rangle_a}{\langle\tau\rangle_a} = 1 + \sum f_i\tau_{0i}k_{qi}[Q] = 1 + K_{SV}^{av}[Q]$$

where K_{SV}^{av} is an intensity-averaged quenching constant. It should be emphasized that the amplitude-averaged, not intensity-averaged, lifetime is a linear function of steady-state fluorescence intensity. For the dynamic component of quenching, $F_0/F = \langle\tau_0\rangle_a/\langle\tau\rangle_a$. Therefore, the use of intensity-averaged lifetimes to calculate the average values of bimolecular collisional rate constants is clearly justified. The data were fit with the nonlinear least-squares method using OriginPro version 8 (OriginLab Corp., Northampton, MA).

Calculation of pK_a Values from Fluorescence λ_{max} Data of the Single-Trp Mutant of TL. Data were analyzed with the assumption that pH-dependent changes in fluorescence λ_{max} are driven mainly by the ionization state of titratable amino acid side chains in the proximity of the tested Trp position. Data strongly support (see below) the validity of this assumption. Therefore, pH titration data were analyzed by fitting the function derived from the Henderson−Hasselbalch equation for multiple titratable groups (*41*):

$$\lambda_{obs}^{max} = \lambda_{min}^{max} + \sum_i \frac{\Delta\lambda_i^{max} \times 10^{pH-pK_i}}{1 + 10^{pH-pK_i}}$$

where λ_{obs}^{max} is the observed fluorescence λ_{max} value at any pH, λ_{min}^{max} is the λ_{max} at the minimum pH value, and $\Delta\lambda_i^{max}$ is the fluorescence λ_{max} difference due to titration of the particular group (or groups with similar pK_a values) assigned by subscript. This equation assumes a noninteracting model with a rapid equilibrium between protonated and unprotonated groups. Data were fit to the formula given above using OriginPro version 8 with the nonlinear least-squares method.

The side chain pK_a values and free energy of unfolding of TL as a function of pH were calculated using PROPKA (*42*) using the coordinates of TL (Protein Data Bank entry 1XKI). Missing loop fragments (part of the AB and GH loops) were modeled using DeepView/Swiss-PdbViewer version 3.7 (GlaxoSmithKline R&D) in accord with solution structure data (*2*).

RESULTS AND DISCUSSION

The fluorescence quantum yield and the lifetime of Trp, as a free amino acid in solution, are invariant in the pH range between 3.0 and 8.5 (*43*, *44*). On the other hand, in proteins, fluorescence parameters of Trp are sensitive to the charge distribution around

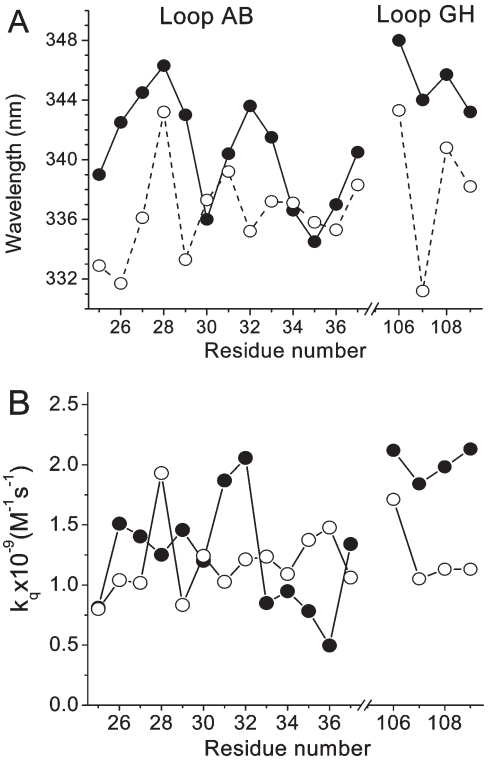

FIGURE 2: Fluorescence λ_{max} (A) and bimolecular quenching rate constants (acrylamide) (B) for the single Trp positioned in the AB and GH loops at pH 7.3 (●) and 3.0 (○). Fluorescence λ_{max} values are determined from the corrected spectra.

the indole ring. Therefore, Trp is an ideal "reporter" group for studying the conformational changes within the pH range of 3.0−8.5. TL shows pH-dependent ligand binding and conformational changes (*23*, *24*, *26*). Specifically, pH regulates the distance between the EF and CD loops in TL (*24*). However, the other two loops at the open end of the barrel have not yet been investigated. Therefore, SDTF was applied to the AB and GH loops for interrogation of pH-induced conformational changes relevant to ligand binding. A single Trp residue, a reporter group, was introduced at various positions of TL as shown in Figure 1.

Side Chain Accessibility of the AB and GH Loop Residues in the Low-pH Transition. Fluorescence parameters

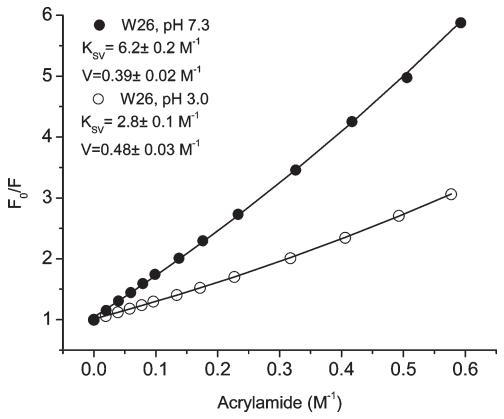

FIGURE 3: Acrylamide quenching of the single-Trp mutant of TL (W26 as an example) at pH 7.3 and 3.0.

Table 1: Fluorescence Lifetime Parameters for Single-Trp Mutants of TL

Trp mutant	α_1	α_2	τ_1 (ns)	τ_2 (ns)	τ^{av} (ns)	$\langle\tau\rangle$ (ns)	K_{SV} (M^{-1})	k_q ($\times10^{-9}$ M^{-1} s^{-1})	V (M^{-1})	Q	χ^2
W25, pH 7.3	0.49	0.51	2.10	5.16	4.30	3.66	3.5	0.81	0.18	0.10	1.1
W25, pH 3.0	0.62	0.38	1.17	4.20	3.26	2.32	2.6	0.80	0.62	0.08	1.3
W26, pH 7.3	0.62	0.38	2.12	5.39	4.11	3.36	6.2	1.51	0.39	0.11	1.0
W26, pH 3.0	0.65	0.35	0.80	3.48	2.68	1.74	2.8	1.04	0.48	0.08	1.6
W27, pH 7.3	0.37	0.63	1.57	6.34	5.73	4.58	8	1.40	0.72	0.15	1.1
W27, pH 3.0	0.68	0.32	1.11	4.03	2.95	2.04	3.0	1.02	0.67	0.07	1.5
W28, pH 7.3	0.40	0.60	0.93	4.50	4.07	3.07	5.1	1.25	0.79	0.13	1.1
W28, pH 3.0	0.64	0.36	0.84	3.49	2.70	1.79	5.2	1.93	0.94	0.07	1.4
W30, pH 7.3	0.65	0.35	0.80	3.38	2.59	1.70	3.1	1.20	0.35	0.07	1.0
W30, pH 3.0	0.74	0.26	1.42	4.16	2.82	2.13	3.5	1.24	0.94	0.07	1.8
W31, pH 7.3	0.68	0.32	1.05	4.12	3.05	2.03	5.7	1.87	0.66	0.10	1.6
W31, pH 3.0	0.69	0.31	1.13	3.80	2.73	1.96	2.8	1.03	1.35	0.06	1.1
W32, pH 7.3	0.65	0.35	1.24	4.69	3.55	2.45	7.3	2.06	0.65	0.11	1.2
W32, pH 3.0	0.62	0.38	0.94	3.80	2.97	2.03	3.6	1.21	1.29	0.08	1.5
W33, pH 7.3	0.50	0.50	1.19	3.70	3.09	2.45	2.8	0.91	0.47	0.10	1.0
W33, pH 3.0	0.67	0.33	0.85	3.57	2.67	1.75	3.3	1.24	1.58	0.07	1.9
W34, pH 7.3	0.43	0.57	0.92	3.83	3.38	2.58	3.6	1.07	0.3	0.12	1.2
W34, pH 3.0	0.77	0.23	1.54	5.05	3.30	2.35	3.6	1.09	0.64	0.08	1.2
W35, pH 7.3	0.27	0.73	1.10	4.28	4.00	3.42	3.2	0.80	0.29	0.13	0.9
W35, pH 3.0	0.60	0.40	1.24	4.55	3.59	2.56	4.9	1.36	0.63	0.12	0.7
W36, pH 7.3	0.45	0.55	1.40	4.73	4.08	3.23	1.8	0.44	0.43	0.12	1.1
W36, pH 3.0	0.74	0.26	1.34	4.21	2.83	2.09	4.2	1.48	0.66	0.08	1.0
W37, pH 7.3	0.65	0.35	0.77	3.89	3.05	1.86	4.1	1.34	0	0.02	1.1
W37, pH 3.0	0.66	0.34	1.19	4.39	3.30	2.28	3.5	1.06	0.84	0.07	1.8
W106, pH 7.3	0.38	0.62	1.16	3.56	3.16	2.65	6.7	2.12	0.81	0.10	0.9
W106, pH 3.0	0.59	0.41	1.01	3.33	2.63	1.96	4.5	1.71	0	0.07	1.3
W107, pH 7.3	0.44	0.56	1.08	5.07	4.50	3.31	8.1	1.80	0.6	0.12	0.9
W107, pH 3.0	0.83	0.17	0.80	3.41	2.00	1.24	2.1	1.05	0	0.06	1.8
W108, pH 7.3	0.41	0.59	0.80	4.55	4.14	3.01	8.8	2.13	0.14	0.10	1.0
W108, pH 3.0[a]	0.50; 0.41	0.08	0.47; 2.16	5.64	2.92	1.58	3.3	1.13	0	0.07	1.3

[a]Three lifetime components were necessary for sufficient fitting.

(intensity, λ_{max}, lifetimes, etc.) of Trp are sensitive to its immediate environment (*46*). Theoretical studies have predicted that upon excitation of Trp, electron density shifts from the pyrrole ring to the benzene ring (*45*). As a consequence, a positive charge near the benzene end or a negative charge near the pyrrole end of the Trp induces a red shift in fluorescence λ_{max} (*45*). Conversely, charges with opposite signs will generate a blue shift in fluorescence λ_{max}.Therefore, each Trp is expected to probe its microscopic electrostatic environment. The fluorescence λ_{max} values of single-Trp mutants at pH 7.3 and 3.0 are shown in Figure 2A. In some positions, e.g., 25, 26, 27, 107, etc., the emission peaks are significantly blue-shifted. Such hypsochromic shifts usually indicate decreased accessibilities (more buried) for the respective side chains of Trp. However, charged residues around the side chain of Trp may give a false impression of decreased accessibility. In any case, a significant shift in fluorescence λ_{max} indicates substantial changes in the environment of the Trp side chain. To detect conformational changes, which result in changes in accessibility to solvent molecules, experiments with acrylamide fluorescence quenching were performed at pH 7.3 and 3.0 (Figures 2B and 3). Bimolecular quenching constants, k_q, calculated from K_{SV} (see Materials and Methods), and fluorescence lifetime data are summarized in Table 1. The low-pH transition significantly changes fluorescence parameters of single Trp residues positioned in both loops. Fluorescence quantum yields and lifetimes are mostly decreased at pH 3.0 compared to that of pH 7.3. Qualitatively, this outcome can be understood from quenching properties of certain amino acids. Glu, Asp, and His (pK_a values of 3.8, 4.5, and 6.5, respectively, in model compounds) are effective quenchers only in protonated states (*47*). Therefore, protonation of these side chains, which are in the proximity of the indole ring of Trp, will enhance fluorescence quenching. In the low-pH transition, the changes in accessibility for the residues of the AB and GH loops are quite different. In the GH loop, all residues show decreased accessibilities, which are consistent with a transition to the "closed" conformation (Figure 2B). The fluorescence λ_{max} values follow the same pattern observed for the accessibility data. All Trp residues positioned in the GH loop show blue-shifted emission in the low-pH transition (Figure 2A). In contrast, the residues located in the AB loop show both decreased and increased accessibilities (Figure 2B). In the low-pH transition, fluorescence λ_{max} values of Trp residues located in the AB loop show mostly blue-shifted emission and have a somewhat different pattern compared to the accessibility data. The average accessibility of the residues in the GH loop is decreased ~38%, from 2.1×10^9 to 1.3×10^9 M^{-1} s^{-1}, with the transition in pH from 7.3 to 3.0. However, in the same transition, despite the significant changes in accessibilities for some residues in the AB loop, the average accessibility per residue remained unchanged [average $k_q = 1.2$ M^{-1} s^{-1} (from Table 1)]. The AB loop is the longest loop in the lipocalin family. Unlike the GH loop, conformational changes observed for the AB loop are not consistent with simple loop motion that just closes over the cavity. More likely, at pH 3.0, the loop assumes the conformation that reshuffles the accessibility profile of some residues. Previously, it has been noted that the AB loop could be a portal region and constituent of the excited protein states for ligand binding (*15*). These findings suggest that various conformations of the AB loop in the excited protein states may be regulated by the protonation state of residues within and/or around that loop.

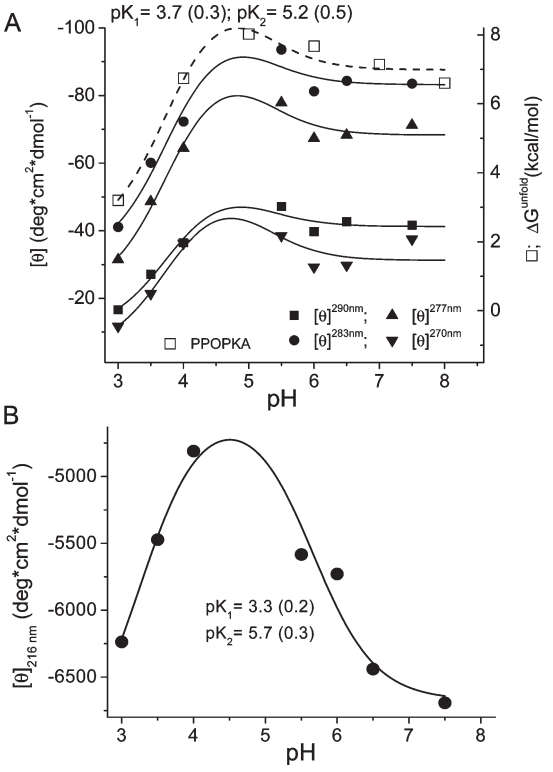

FIGURE 4: (A) Molar ellipticities at λ values of 270, 277, 283, and 290 nm (from near-UV CD) and free energy unfolding (calculated using PROPKA) for TL at various pH values. Lines are generated by a global analysis of the data with a two-component pH titration curve where pK values are assigned as global parameters. (B) Molar ellipticity at a λ of 216 nm (from far-UV CD) for TL at various pH values. CD data points are from ref *24*.

Global Structural Transition of TL during pH Titration. CD pH titration experiments were performed to characterize global structural transitions of TL. Near-UV CD spectra of proteins are sensitive to both spatial arrangement and asymmetry (mobility) of its aromatic residues (*48*). Therefore, the near-UV CD spectrum is unique for each protein and reflects the overall conformational state. The intensities of the near-UV CD spectrum of TL at λ values of 270, 277, 283, and 290 nm as a function of pH are shown in Figure 4A. Decreased CD intensities indicate conformational relaxation of TL. Despite the fact that the contributions of the aromatic residues (Phe, Tyr, and Trp) are different at the selected wavelengths, all of them show a similar pattern and could be fit with global parameters. Two pK_a values, 3.7 and 5.2, are apparent from pH titration in the near-UV CD (Figure 4A). The pH titration experiment in far-UV CD yields similar pK_a values, 3.3 and 5.7 (Figure 4B). Concordance of pH titration data in near- and far-UV CD indicates that the pH-induced structural transitions are cooperative. A previous CD study has shown that the secondary structure of TL does not change significantly at pH 3.0 (*24*, *26*). However, near-UV CD of TL shows significantly diminished intensity at this pH value. ANS binding to TL at various pH values (7.5−2.0) shows that the ANS fluorescence enhancement reaches its maximum value at pH 3.0 and then sharply decreases (*24*). Enhanced ANS binding at low pH (3.0) is consistent with a molten globule transition (*23*, *24*, *26*). Therefore, pK_a values of 3.3−3.7, which were obtained from CD pH titration experiments (Figure 4), can be considered as the pK_a for this transition. pH decreased from 7.5 to 5.0 results in the enhanced near-UV CD intensities for TL

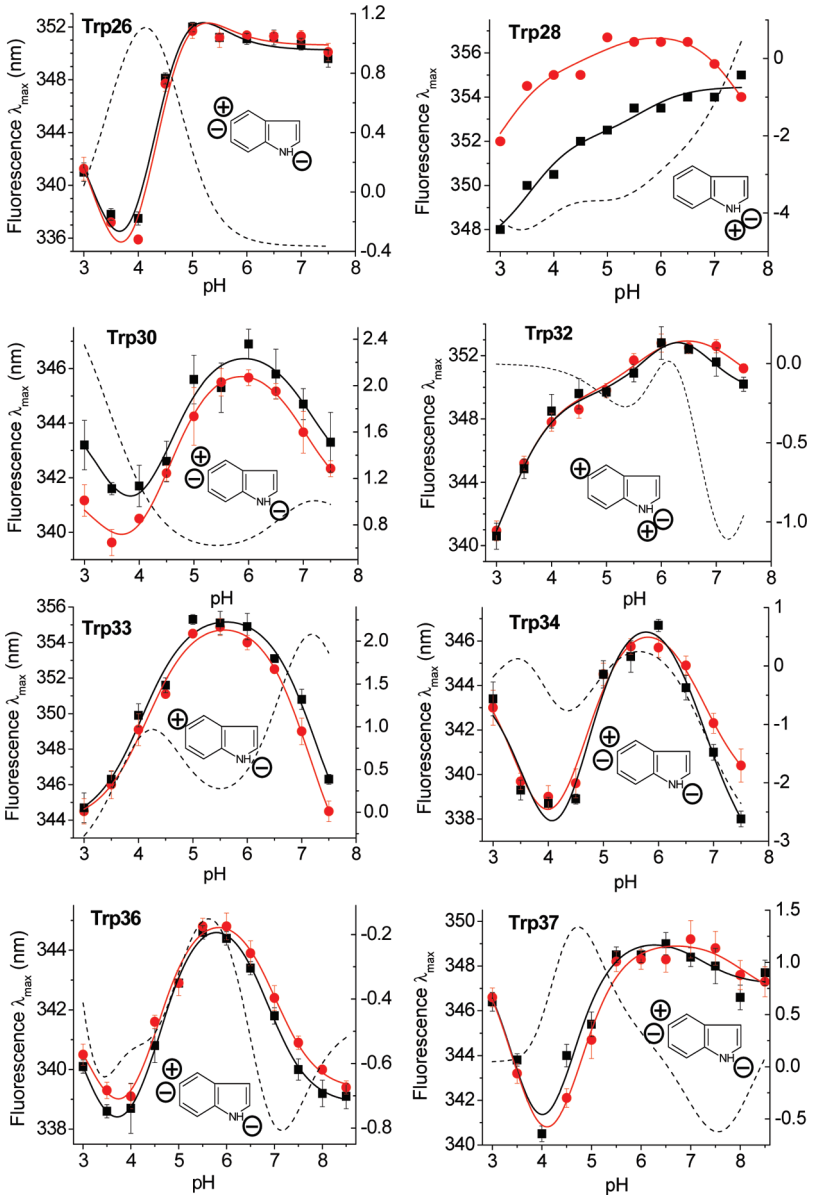

FIGURE 5: Fluorescence λ_{max} data as a function of pH for single-Trp mutants of the AB loop. Red and black symbols represent data for apo- and holoproteins, respectively. Solid lines are fitting curves for two or three titratable groups (see Materials and Methods). Dashed lines (right *y*-axis) are difference titration curves (holo minus apo). To eliminate additional uncertainty in titration experiments, fluorescence λ_{max} values are taken from the uncorrected (only corrected for buffer scattering) spectra. The insets show models for apparent charge distributions around the indole ring of Trp consistent with experimental data. pK_a values of > 5.0 were modeled as a positive charge. The effect of the charged group (positive or negative) localized around the indole ring on the fluorescence λ_{max} is described in the text.

(Figure 4A), which are suggestive of the more rigid conformations. It should be noted that there is an apparent disagreement between near- and far-UV CD results. A decrease in pH from 7.5 to 4.5 results in the diminished far-UV CD intensities (λ = 216 nm), which usually suggest unfolding of the protein. However, close inspection of the far-UV CD spectra of TL at various pH values (in ref *24*) shows that the apparent decreases in the far-UV CD intensities are the result of an overall spectral shift with almost the same spectral shape and intensity. As a result, the ratios of the CD intensities, positive to negative, are increased. It has been shown that an increase in the degree of twist in β-sheets generates an increased $|\theta_{\pi\pi^*}|/|\theta_{n\pi^*}|$, i.e., ratio of positive to negative peaks. This parameter has been suggested as a criterion for the degree of twisting in β-sheets (*49*). A right-hand twist of β-sheets lowers the free energy (*50*) and, therefore, increases the protein stability. Thus, the pH titration data obtained from the far-UV CD corroborate those of the near-UV CD. The data suggest that TL undergoes a transition (p$K_a \sim 5.7$), which results in a more rigid conformation. The isoelectric point of TL is at ~4.5−5.4 (*32*). The pH titration data (Figure 4) indicate that more balanced charge distribution (pH value close to pI) enhances the stability of TL. Unfolding free energies of TL at various pH values, calculated using PROPKA (*42*), match pH titration data obtained with CD (Figure 4). In fact, both near-UV CD and PROPKA data could be fitted to a two-component pH titration curve with pK_a values assigned as global parameters (Figure 4A). It is to be noted that neither near-UV CD nor far-UV CD is sensitive to the loop conformation unless it has secondary structure elements. Therefore, the results of pH titration data of TL obtained by CD spectroscopy convey the global structural transitions associated with the secondary structure and are not specific for this particular part of the protein.

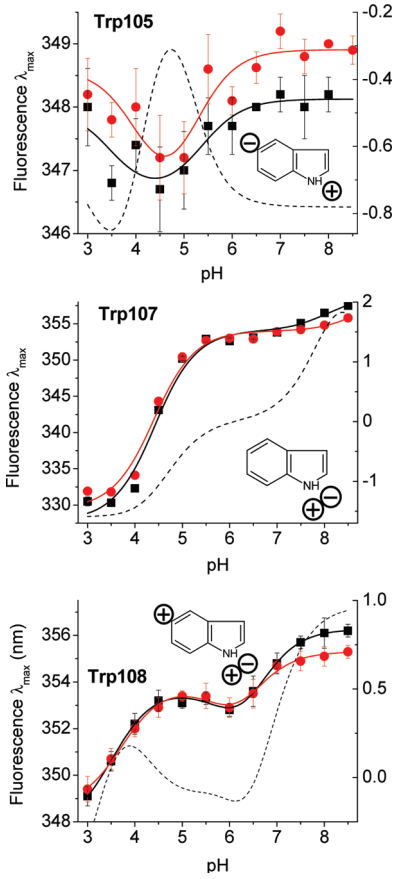

FIGURE 6: Fluorescence λ_{max} values as a function of pH for single-Trp mutants of the GH loop. Red and black symbols represent data for apo- and holoproteins, respectively. Solid lines are fitting curves for two or three titratable groups (see Materials and Methods). Dashed lines (right *y*-axis) are difference titration curves (holo minus apo). The insets are the same as those in Figure 5.

Site-Specific pH Titration of TL by Fluorescence of Trp Residues Positioned in the AB and GH Loops. Fluorescence and accessibility parameters of Trp positioned in the AB and GH loops indicate conformational changes in the transition to low pH. CD spectroscopy reveals two global structural transitions (pK_a values of ~3.5 and ~5.7). However, the secondary structure of TL is essentially intact up to pH 3.5 (*24*). Since the Trp fluorescence λ_{max} is most sensitive to its nearest charge distribution, pH titration could reveal the mechanism of the conformational transition in the loops. Fluorescence λ_{max} values of selected Trp residues as a function of pH for the AB and GH loops are shown in Figures 5 and 6, respectively. Because the fluorescence titration curves differ from each other, as well as from CD titration curves (Figure 4), the data strongly support the idea that pH titration curves are position-dependent and, therefore, reflect the immediate environment of each Trp residue (Figures 5 and 6). pK_a values for each transition are listed in Table 2. For comparison, pK_a values of the titratable groups, as predicted by PROPKA, are listed in Table 3. Up to three distinct pK_a values could be identified. Saturation of TL by palmitic acid (holoproteins) generates significant changes to the titration behavior of the amino acids around Trp28 (Figure 5). Differences in protonation states between the holo and apo forms of the protein with a single Trp in other positions are not apparent, with the exception of Trp37. Interestingly, both residues, at positions 28 and 37, are positioned in the flanking region of the AB loop.

Table 2: pK_a Values for Apo and Holo Forms of Single-Trp Mutants of TL Determined from Fluorescence pH Titration Data (Figures 5 and 6)

	pK_{a1} ± standard deviation	pK_{a2} ± standard deviation	pK_{a3} ± standard deviation
apoW26	3.5[a]	4.3 ± 0.5	4.9 ± 0.8
holoW26	3.5[a]	4.3 ± 0.5	5.0 ± 0.8
apoW28	3.0 ± 0.3	4.9 ± 1.2	7.5 ± 1.0
holoW28	3.5 ± 0.2	5.7 ± 0.6	–
apoW30	3.4 ± 0.3	4.5 ± 0.2	7.0 ± 0.4
holoW30	3.4 ± 0.3	4.5 ± 0.3	7.1 ± 0.4
apoW32	3.2 ± 0.2	5.6 ± 0.4	7.4 ± 1.2
holoW32	3.2 ± 0.2	6.0 ± 1.1	6.6 ± 1.1
apoW33	–	4.2 ± 0.1	7.1 ± 0.2
holoW33	–	4.1 ± 0.1	7.3 ± 0.2
apoW34	3.6 ± 0.4	4.5 ± 0.4	6.8 ± 0.4
holoW34	3.9 ± 0.6	4.4 ± 0.6	6.8 ± 0.3
apoW36	3.3 ± 0.6	4.5 ± 0.2	7.0 ± 0.1
holoW36	3.0 ± 0.8	4.6 ± 0.2	6.9 ± 0.1
apoW37	3.6 ± 0.3	4.6 ± 0.3	8.0 ± 1.0
holoW37	3.6 ± 0.3	4.4 ± 0.4	7.2 ± 0.7
apoW105	4.1 ± 0.6	5.1 ± 0.6	–
holoW105	3.5 ± 0.5	5.3 ± 0.5	–
apoW107	–	4.4 ± 0.1	8.9[b] ± 6.4
holoW107	–	4.4 ± 0.1	8.1 ± 1.1
apoW108	3.7 ± 0.1	6.2 ± 1.6	6.2 ± 0.5
holoW108	3.5 ± 0.1	6.2 ± 1.6	6.4 ± 1.0

[a]Fixed value. [b]Low-accuracy value.

Table 3: pK_a Values of Titratable Groups Relevant to Ligand Binding for TL As Predicted with PROPKA[a]

amino acid	pK_a(apo) from PROPKA	pK_a from model
Asp25	3.21	3.8
Glu27	4.61	4.50
Glu30	6.44	4.50
Glu34	3.85	4.50
Glu102	3.91	4.50
Glu104	4.89	4.50
Glu142	5.37	4.50
His84	10.26	6.50
His96	7.51	6.50
His106	6.29	6.50

[a]The atomic coordinates for calculations of pK_a values were taken from Protein Data Bank entry 1xki.

The data suggest that fluctuation of the protonation state around these residues (particularly around residue 28) triggers conformational rearrangement of the AB loop that influences ligand binding. For the GH loop, no obvious shifts could be observed in pH titration curves between the holo and apo form of the proteins. Since variation in fluorescence λ_{max} values is linked to the accessibility data (Figure 2), a vertical shift in the pH titration data could be associated with the amplitude of movement of the loops. While mutations of charged residues could disturb electrostatic interactions, native residues at positions 28 and 37 are uncharged, Phe and Thr, respectively. Therefore, in the most significant case, the mutant Trp28 reports conformational changes where protonation states of adjacent residues are not perturbed. Regardless of the nature of the conformational transition of the AB loop, a significant shift in the pH titration curves of apo- and holo-W28 indicates that the electrostatic interactions around this residue are stabilized by ligand binding and, therefore, functionally significant.

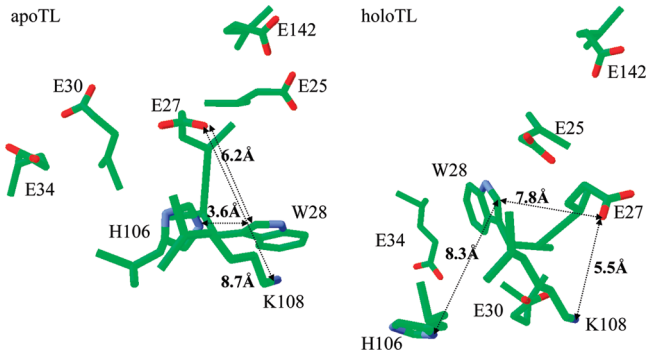

FIGURE 7: Distribution of relevant charged residues around Trp28 (F28W mutant) in apo- and holo-TL, coordinates of which were taken from Protein Data Bank entries 1XKI and 3EYC, respectively. Molecules were superimposed using DeepView/Swiss-PdbViewer version 3.7 (GlaxoSmithKline R&D), which included 109 atoms (root-mean-square deviation of 1.2 Å). Color coding: green for backbone and carbon atoms, red for oxygens, and blue for nitrogens.

Note Added after Submission. The crystal structure of holo-TL (*51*), which became available after the submission of this work, corroborates our findings. The spatial distributions of the relevant amino acids around the "reporter" Trp28 in apo- and holo-TL are informative (Figure 7). It has been suggested that electrostatic contact between residues Glu27 and Lys108, which are located in the neighboring AB and GH loops, fixes the open conformation of the AB loop for ligand binding (*51*). Indeed, in holo-TL, the distance between amino acids Glu27 and K108 (OE1 and NA, respectively) decreases to 5.5 Å compared to that of apo-TL (8.7 Å). The relative orientations and distances of the side chains of relevant amino acides around Trp 28 are noticeably different in holo- versus apo-TL (Figure 7). The significant difference between titration curves of apo-W28 and holo-W28 (Figure 5) found in solution corroborates findings from the crystal structures of apo- and holo-TL. Therefore, it is reasonable to suggest that fluctuations of the protonation states of these titratable groups, particularly E27, regulate ligand binding and define the pH dependence of the ligand binding. Because of the complexity of the charge distribution, additional experimental data are necessary to assign the relative contributions of the titratible groups into the pH titration curves of holo- and apo-W28. Previously, it has been shown that some mutations, notably, E27W and K108W, decrease the affinities of palmitic acid for TL (*15*). These results also corroborate the independently proposed mechanism (this work and ref *51*). In both mutations, electrostatic interaction between residues E27 and K108, which fixes the open conformation for ligand binding, will be disrupted.

The findings demonstrate that SDTF provides a promising approach to the study of the solution structure of proteins, as well as pH-dependent conformational dynamics, that is highly complementary to structural methods such as crystallography.

REFERENCES

1. Flower, D. R. (1996) The lipocalin protein family: Structure and function. *Biochem. J. 318* (Part 1), 1–14.
2. Gasymov, O. K., Abduragimov, A. R., Yusifov, T. N., and Glasgow, B. J. (2001) Site-directed tryptophan fluorescence reveals the solution structure of tear lipocalin: Evidence for features that confer promiscuity in ligand binding. *Biochemistry 40*, 14754–14762.
3. Breustedt, D. A., Korndorfer, I. P., Redl, B., and Skerra, A. (2005) The 1.8-Å crystal structure of human tear lipocalin reveals an extended branched cavity with capacity for multiple ligands. *J. Biol. Chem. 280*, 484–493.
4. Glasgow, B. J., Abduragimov, A. R., Farahbakhsh, Z. T., Faull, K. F., and Hubbell, W. L. (1995) Tear lipocalins bind a broad array of lipid ligands. *Curr. Eye Res. 14*, 363–372.
5. Glasgow, B. J., Marshall, G., Gasymov, O. K., Abduragimov, A. R., Yusifov, T. N., and Knobler, C. M. (1999) Tear lipocalins: Potential lipid scavengers for the corneal surface. *Invest. Ophthalmol. Visual Sci. 40*, 3100–3107.
6. Selsted, M. E., and Martinez, R. J. (1982) Isolation and purification of bactericides from human tears. *Exp. Eye Res. 34*, 305–318.
7. van't Hof, W., Blankenvoorde, M. F., Veerman, E. C., and Amerongen, A. V. (1997) The salivary lipocalin von Ebner's gland protein is a cysteine proteinase inhibitor. *J. Biol. Chem. 272*, 1837–1841.
8. Blaker, M., Kock, K., Ahlers, C., Buck, F., and Schmale, H. (1993) Molecular cloning of human von Ebner's gland protein, a member of the lipocalin superfamily highly expressed in lingual salivary glands. *Biochim. Biophys. Acta 1172*, 131–137.
9. Redl, B., Holzfeind, P., and Lottspeich, F. (1992) cDNA cloning and sequencing reveals human tear prealbumin to be a member of the lipophilic-ligand carrier protein superfamily. *J. Biol. Chem. 267*, 20282–20287.
10. Lechner, M., Wojnar, P., and Redl, B. (2001) Human tear lipocalin acts as an oxidative-stress-induced scavenger of potentially harmful lipid peroxidation products in a cell culture system. *Biochem. J. 356*, 129–135.
11. Glasgow, B. J., Abduragimov, A. R., Gassymov, O. K., Yusifov, T. N., Ruth, E. C., and Faull, K. F. (2002) Vitamin E associated with the lipocalin fraction of human tears. *Adv. Exp. Med. Biol. 506*, 567–572.
12. Yusifov, T. N., Abduragimov, A. R., Gasymov, O. K., and Glasgow, B. J. (2000) Endonuclease activity in lipocalins. *Biochem. J. 347* (Part 3), 815–819.
13. Gasymov, O. K., Abduragimov, A. R., Yusifov, T. N., and Glasgow, B. J. (2000) Resolution of ligand positions by site-directed tryptophan fluorescence in tear lipocalin. *Protein Sci. 9*, 325–331.
14. Glasgow, B. J., Gasymov, O. K., Abduragimov, A. R., Yusifov, T. N., Altenbach, C., and Hubbell, W. L. (1999) Side chain mobility and ligand interactions of the G strand of tear lipocalins by site-directed spin labeling. *Biochemistry 38*, 13707–13716.
15. Gasymov, O. K., Abduragimov, A. R., and Glasgow, B. J. (2009) Intracavitary Ligand Distribution in Tear Lipocalin by Site-Directed Tryptophan Fluorescence. *Biochemistry 48*, 7219–7228.
16. Okazaki, K., and Takada, S. (2008) Dynamic energy landscape view of coupled binding and protein conformational change: Induced-fit versus population-shift mechanisms. *Proc. Natl. Acad. Sci. U.S.A. 105*, 11182–11187.
17. Eberini, I., Baptista, A. M., Gianazza, E., Fraternali, F., and Beringhelli, T. (2004) Reorganization in apo- and holo-β-lactoglobulin upon protonation of Glu89: Molecular dynamics and pK_a calculations. *Proteins 54*, 744–758.
18. Fogolari, F., Ragona, L., Licciardi, S., Romagnoli, S., Michelutti, R., Ugolini, R., and Molinari, H. (2000) Electrostatic properties of bovine β-lactoglobulin. *Proteins 39*, 317–330.
19. Ragona, L., Fogolari, F., Catalano, M., Ugolini, R., Zetta, L., and Molinari, H. (2003) EF loop conformational change triggers ligand binding in β-lactoglobulins. *J. Biol. Chem. 278*, 38840–38846.
20. Sakurai, K., Konuma, T., Yagi, M., and Goto, Y. (2009) Structural dynamics and folding of β-lactoglobulin probed by heteronuclear NMR. *Biochim. Biophys. Acta 1790*, 527–537.
21. Fogolari, F., Moroni, E., Wojciechowski, M., Baginski, M., Ragona, L., and Molinari, H. (2005) MM/PBSA analysis of molecular dynamics simulations of bovine β-lactoglobulin: Free energy gradients in conformational transitions? *Proteins 59*, 91–103.
22. Prats, M., Teissie, J., and Tocanne, J. F. (1986) Lateral proton conduction at lipid−water interfaces and its implications for the chemiosmotic-coupling hypothesis. *Nature 322*, 756–758.
23. Gasymov, O. K., Abduragimov, A. R., and Glasgow, B. J. (2007) Molten globule state of tear lipocalin: ANS binding restores tertiary interactions. *Biochem. Biophys. Res. Commun. 357*, 499–504.
24. Gasymov, O. K., Abduragimov, A. R., Yusifov, T. N., and Glasgow, B. J. (2004) Interstrand loops CD and EF act as pH-dependent gates to regulate fatty acid ligand binding in tear lipocalin. *Biochemistry 43*, 12894–12904.
25. Gasymov, O. K., Abduragimov, A. R., Gasimov, E. O., Yusifov, T. N., Dooley, A. N., and Glasgow, B. J. (2004) Tear lipocalin: Potential for selective delivery of rifampin. *Biochim. Biophys. Acta 1688*, 102–111.
26. Gasymov, O. K., Abduragimov, A. R., Yusifov, T. N., and Glasgow, B. J. (1998) Structural changes in human tear lipocalins associated with lipid binding. *Biochim. Biophys. Acta 1386*, 145–156.

27. Calderone, V., Berni, R., and Zanotti, G. (2003) High-resolution structures of retinol-binding protein in complex with retinol: pH-induced protein structural changes in the crystal state. *J. Mol. Biol. 329*, 841–850.
28. Newcomer, M. E., and Ong, D. E. (2000) Plasma retinol binding protein: Structure and function of the prototypic lipocalin. *Biochim. Biophys. Acta 1482*, 57–64.
29. Roberts, S. A., Weichsel, A., Qiu, Y., Shelnutt, J. A., Walker, F. A., and Montfort, W. R. (2001) Ligand-induced heme ruffling and bent no geometry in ultra-high-resolution structures of nitrophorin 4. *Biochemistry 40*, 11327–11337.
30. Hwang, P. M., Choy, W. Y., Lo, E. I., Chen, L., Forman-Kay, J. D., Raetz, C. R., Prive, G. G., Bishop, R. E., and Kay, L. E. (2002) Solution structure and dynamics of the outer membrane enzyme PagP by NMR. *Proc. Natl. Acad. Sci. U.S.A. 99*, 13560–13565.
31. Glasgow, B. J., Heinzmann, C., Kojis, T., Sparkes, R. S., Mohandas, T., and Bateman, J. B. (1993) Assignment of tear lipocalin gene to human chromosome 9q34-9qter. *Curr. Eye Res. 12*, 1019–1023.
32. Glasgow, B. J. (1995) Tissue expression of lipocalins in human lacrimal and von Ebner's glands: Colocalization with lysozyme. *Graefe's Arch. Clin. Exp. Ophthalmol. 233*, 513–522.
33. Cormack, B. (1987) in Current Protocols in Molecular Biology, Suppl. 15, Greene Publishing Associates and Wiley-Interscience, New York.
34. Gasymov, O. K., Abduragimov, A. R., Yusifov, T. N., and Glasgow, B. J. (1999) Binding studies of tear lipocalin: The role of the conserved tryptophan in maintaining structure, stability and ligand affinity. *Biochim. Biophys. Acta 1433*, 307–320.
35. Bozimowski, D., Artiss, J. D., and Zak, B. (1985) The variable reagent blank: Protein determination as a model. *J. Clin. Chem. Clin. Biochem. 23*, 683–689.
36. Peterson, G. L. (1977) A simplification of the protein assay method of Lowry et al. which is more generally applicable. *Anal. Biochem. 83*, 346–356.
37. Gasymov, O. K., Abduragimov, A. R., Yusifov, T. N., and Glasgow, B. J. (1997) Solution structure by site directed tryptophan fluorescence in tear lipocalin. *Biochem. Biophys. Res. Commun. 239*, 191–196.
38. Eftink, M. R., and Ghiron, C. A. (1976) Exposure of tryptophanyl residues in proteins. Quantitative determination by fluorescence quenching studies. *Biochemistry 15*, 672–680.
39. Sillen, A., and Engelborghs, Y. (1998) The Correct Use of "Average" Fluorescence Parameters. *Photochem. Photobiol. 67*, 475–486.
40. Gastmans, M., Volckaert, G., and Engelborghs, Y. (1999) Tryptophan microstate reshuffling upon the binding of cyclosporin A to human cyclophilin A. *Proteins 35*, 464–474.
41. Freedman, M. H., Lyerla, J. R., Jr., Chaiken, I. M., and Cohen, J. S. (1973) Carbon-13 nuclear-magnetic-resonance studies on selected amino acids, peptides, and proteins. *Eur. J. Biochem. 32*, 215–226.
42. Li, H., Robertson, A. D., and Jensen, J. H. (2005) Very fast empirical prediction and rationalization of protein pK_a values. *Proteins 61*, 704–721.
43. De Lauder, W. B., and Wahl, P. (1970) pH dependence of the fluorescence decay of tryptophan. *Biochemistry 9*, 2750–2754.
44. Liu, B., Thalji, R. K., Adams, P. D., Fronczek, F. R., McLaughlin, M. L., and Barkley, M. D. (2002) Fluorescence of cis-1-amino-2-(3-indolyl)cyclohexane-1-carboxylic acid: A single tryptophan χ_1 rotamer model. *J. Am. Chem. Soc. 124*, 13329–13338.
45. Vivian, J. T., and Callis, P. R. (2001) Mechanisms of tryptophan fluorescence shifts in proteins. *Biophys. J. 80*, 2093–2109.
46. Lakowicz, J. R. (2006) Principles of Fluorescence Spectroscopy, 3rd ed., Springer, New York.
47. Chen, Y., and Barkley, M. D. (1998) Toward understanding tryptophan fluorescence in proteins. *Biochemistry 37*, 9976–9982.
48. Fasman, G. D., Ed. (1996) Circular dichroism and the conformational analysis of biomolecules, Plenum Press, New York.
49. Woody, R. W. (1996) Theory of Circular Dichroism of Proteins. In Circular Dichroism and the Conformational Analysis of Biomolecules (Fasman, G. D., Ed.) p 55, Plenum Press, New York.
50. Chothia, C. (1973) Conformation of twisted β-pleated sheets in proteins. *J. Mol. Biol. 75*, 295–302.
51. Breustedt, D. A., Chatwell, L., and Skerra, A. (2009) A new crystal form of human tear lipocalin reveals high flexibility in the loop region and induced fit in the ligand cavity. *Acta Crystallogr. D65*, 1118–1125.